Check for updates

ADVANCED MATERIALS TECHNOLOGIES
www.advmattechnol.de

Femtosecond-Laser-Direct-Writing Micro-Scale Soft Actuators with Controllable Shape Morphing

Yong Wang, Yunlong Li, Jiao Geng, Zhiming Hu, Fengjiang Liu, Liping Shi, Jiu-an Lv, and Min Qiu**

Micro-scale soft actuators with controllable shape-morphing are the focus of advanced technological fields, ranging from advancing sensing, industrial robotics, and digital manufacturing to medical devices. Particularly, there is a growing interest in the scientific community to leverage liquid crystal polymers (LCPs) to fabricate such soft actuators, because LCPs can offer reversible, programmable deformations under external stimuli. However, pattern micromachining of LCPs into micro-scale remains a daunting challenge. Herein, a femtosecond laser direct writing (FsLDW) method for cross-linked LCP (CLCP) microstructure construction is reported that enables arbitrary pattern machining with a minimum size of 40 µm and average heat-affected zone (HAZ) below 8 µm through optimization of processing parameters. Light-driven behaviors of CLCP microstructures are systematically characterized through analyzing the effects of film thickness, length-width ratio, light irradiation time, incident angle, light intensity, and cutting direction on bending and twisting behaviors. Finally, a light-driven micromirror system is demonstrated, which can achieve not only a controllable swing but also a rotation of the mirror surface with a maximum scanning frequency of ≈2 Hz.

1. Introduction

Admiration for nature has fueled the dream of developing man-made materials that have the imitation ability and adaptability of living creatures.[1] Stimuli-responsive materials that can generate complex shape deformation under light irradiation are promising materials for fulfilling this dream as light is clean energy and can be precisely and conveniently manipulated in terms of wavelength, intensity, and polarization direction. They have been developed for various smart actuator applications including medical devices,[2,3] robotics,[4–6] biomimetic devices,[7,8] lab-on-a-chip,[9,10] and micro-opto-electro-mechanical systems (MOEMS),[11–13] because they can convert light energy directly into mechanical work. Among these materials, light-responsive liquid crystal polymers, including liquid crystal networks (LCNs),[14,15] liquid crystal elastomers (LCEs),[16,17] and cross-linked liquid crystal polymers (CLCPs),[18–20] have gained significant attention due to their ease of light-induced actuation in a dry and wet environment and the ability to engineer molecular alignments within the liquid crystal matrix. As a combination of polymer networks and liquid crystals, CLCPs exhibit unique properties such as elasticity, anisotropy, self-assembly, and molecular cooperation effect. The most important property is that the orientation of mesogens is strongly coupled with the conformation of polymer backbones, thus liquid crystal (LC) arrangement change will induce the whole material's macroscopic deformation.[21] For light-driven CLCP actuators, the light response can be either photochemical or photothermal. It has been demonstrated that the CLCPs can undergo large thermal-induced contractions due to the mesogen molecular alignment changes caused by the thermal phase transition from the LC phase to the isotropic phase.[22] In addition, some photo-responsive molecules, such as azobenzenes have been incorporated into the side chains of polymer networks to achieve photochemical-responsive CLCPs.[23–25] Upon irradiation of UV light, *trans-cis* photoisomerization of azobenzenes occurs, then the bent *cis* isomers disturb the alignment of LCs, causing a macroscopic photo-deformation of materials in the form of contraction, bending, swing, twisting and rotation.[22,26] Furthermore, these light-induced deformations

Y. Wang, Y. Li, J. Geng, Z. Hu, F. Liu, L. Shi, J.-an Lv, M. Qiu
Key Laboratory of 3D Micro/Nano Fabrication and Characterization of Zhejiang Province
School of Engineering
Westlake University
Hangzhou 310024, China
E-mail: lvjiuan@westlake.edu.cn; qiu_lab@westlake.edu.cn

Y. Wang
Department of Mechanical Engineering
Hangzhou City University
Hangzhou 310015, China

Y. Wang, Y. Li, J. Geng, Z. Hu, F. Liu, L. Shi, J.-an Lv, M. Qiu
Institute of Advanced Technology
Westlake Institute for Advanced Study
Hangzhou 310024, P. R. China

Y. Li
Department of Materials Science & State Key Laboratory of Molecular Engineering of Polymers
Fudan University
220 Handan Road, Shanghai 200433, P. R. China

M. Qiu
Westlake Institute for Optoelectronics
Hangzhou 311421, P. R. China

The ORCID identification number(s) for the author(s) of this article can be found under https://doi.org/10.1002/admt.202300967

DOI: 10.1002/admt.202300967

 © 2023 Wiley-VCH GmbH

2365709x, 0, Downloaded from https://onlinelibrary.wiley.com/doi/10.1002/admt.202300967 by Zhejiang University, Wiley Online Library on [04/10/2023]. See the Terms and Conditions (https://onlinelibrary.wiley.com/terms-and-conditions) on Wiley Online Library for rules of use; OA articles are governed by the applicable Creative Commons License

have been applied to various soft actuators, including plastic motors,[27] inchworm-like walkers,[28] flexible microrobots,[29] and artificial cilia.[30]

For achieving above applications, it is critical to control the orientation of the mesogens. Photo- and thermal-polymerization of aligned LC molecules in a liquid crystal cell have been widely used for the preparation of freestanding CLCP films with several tens of micrometers in thickness (15 to 60 μm) with different orientations.[31] However, the orientation, molding, and crosslinking in an LC cell determines the size and shape of CLCP films (generally several centimeters long) and constrains the construction of CLCP microstructures for diverse soft micro-actuators. In addition, conventional mechanical machining often suffers from large vibrations, easily causing cracks in CLCP films (due to the mechanical fragility of highly cross-linked networks), thus is not ideal for CLCP film micromachining. As a result, the size of most current CLCP actuators is in millimeter or centimeter level.[32–35] Recently, 3D or 4D printing technologies have been utilized for preparation of liquid crystal elastomer micro-actuators bearing high work capacity and capability of reversible complex shape morphing derived from thermomechanical response for programmed mesogen orientation.[36–39] However, direct printing of uniform CLCP film with higher resolution down to micrometer-scale is still a challenge due to high viscosity in nematic state while printing in isotropic state, although the viscosity is much reduced, leads to materials in polydomain and loss of stimuli-responsive mechanical deformation.[37] Two-photon polymerization is another emerging technology for the fabrication of CLCP which can achieve 3D manufacturing in nanoscale while the orientation of the mesogens is difficult to control.[40,41] Moreover, the printing efficiency is low. Therefore, it is highly desirable for the preparation of CLCP microstructure with a convenient, economical, efficient, and high-resolution method.

Recently, femtosecond laser direct writing has been proven as a powerful 3D micro/nanofabrication method for high accuracy and flexible fabrication of planar or 3D microstructures, including optical waveguides,[42] microfluidics masks,[43] microfluidic chips,[44] microchannels[45] and polymer-based microcavities.[46] Compared to traditional fabrication technology, FsLDW offers several distinct advantages: it is a facile, rapid, non-contact and maskless approach that can realize arbitrary, designable and complicated architectures with a nanometric resolution.[47–51] In addition, due to its high spatial restriction of the laser energy and an fs-scale pulse width that is much shorter than the thermal diffusion time, FsLDW method can provide a lower collateral damage.[49] Besides, FsLDW technologies exhibit a unique property of non-invasiveness, reducing the mechanical vibration effect on flexible CLCP film processing and then enabling high precision, thus being especially suitable for thin film structure micromachining.

In this paper, we provide a femtosecond laser direct writing method for CLCP film microstructure construction by investigating effects of machining parameters (laser pulse duration, power, and scanning speed) on CLCP microstructure HAZ. We have achieved a minimum machining size of 40 μm with an average HAZ of ≈8 μm through optimization of machining parameters. Moreover, we have systematically characterized effects of film thickness, length-width ratio, light irradiation time, incident angle, light intensity, and cutting direction on bending or twisting behaviors of CLCP microstructures. Finally, we fabricate and demonstrate a controllable light-driven CLCP micromirror system, which can realize not only a swing but also a rotation motion, showing great potential for applications of CLCP microstructures for micro-scale light-driven soft actuators with controllable shape morphing.

2. Experimental Section

2.1. CLCP Film Preparation

The chemical structures for preparation of CLCP films are shown in **Figure 1**a, which consist of 78 mol% of the LC monomer 1, 20 mol% of the crosslinker 2, 1 mol% of the dye 3 and 1 mol% of the photoinitiator (Irgacure 369). The CLCP films were fabricated using one-step method developed by Broer et al. in the 1980s,[52] and the schematic illustration of the one-step method to prepare CLCP films is shown in Figure 1b. First, the liquid-crystalline monomer mixtures were heated to an isotropic phase. Then the molten LC monomer mixtures were injected into the LC cell coated with a rubbed polyimide alignment layer by the capillary force and arranged in the preferred rubbing direction due to the surface anchoring effect. The thickness of the CLCP films was controlled by adjusting the spacing of glass cells with spacers. Finally, highly ordered structures of LCs were fixed by photopolymerization. The LC cell could be further opened to produce a uniform and freestanding CLCP film. In this work, CLCP films with parallel and twisted nematic geometry were synthesized by coating different direction orientation agents on the glass substrate, respectively. The thickness of prepared CLCP films is from 15 to 60 μm with an error range below 1 μm. Figure 1c shows the absorbance spectra for parallel nematic and twisted nematic CLCP films, with a sharp and almost non-interfered absorption ≈502 nm and 515 nm, respectively.

2.2. CLCP Film Micromachining

The experimental setup for femtosecond laser direct writing of CLCP microstructure is shown in Figure S1 (Supporting Information). An ultrafast fiber femtosecond laser (Amplitude) delivering a central wavelength of 1030 nm, and a pulse duration of 130 fs was used. The laser beam was attenuated by a neutral density (ND) attenuator to adjust the power. Then the laser beam diameter was expanded to 9 mm by a beam expander. Finally, the expanded laser beam was focused onto the CLCP film through an objective lens with focal length of $f = 20$ mm. The CLCP film was put on a 3D moving platform to realize pattern micromachining. The diameter at the laser focal spot was measured to be ≈3 μm using a CCD camera beam profiler. A CCD camera was utilized for observing the micromachining process. To reduce CLCP microstructure HAZ, the repetition rate of femtosecond laser was set as 0.8 kHz, with a power of 20–25 mW, and the scanning speed for the moving platform was ≈0.4 $mm^{-1}s$ during the machining process.

© 2023 Wiley-VCH GmbH

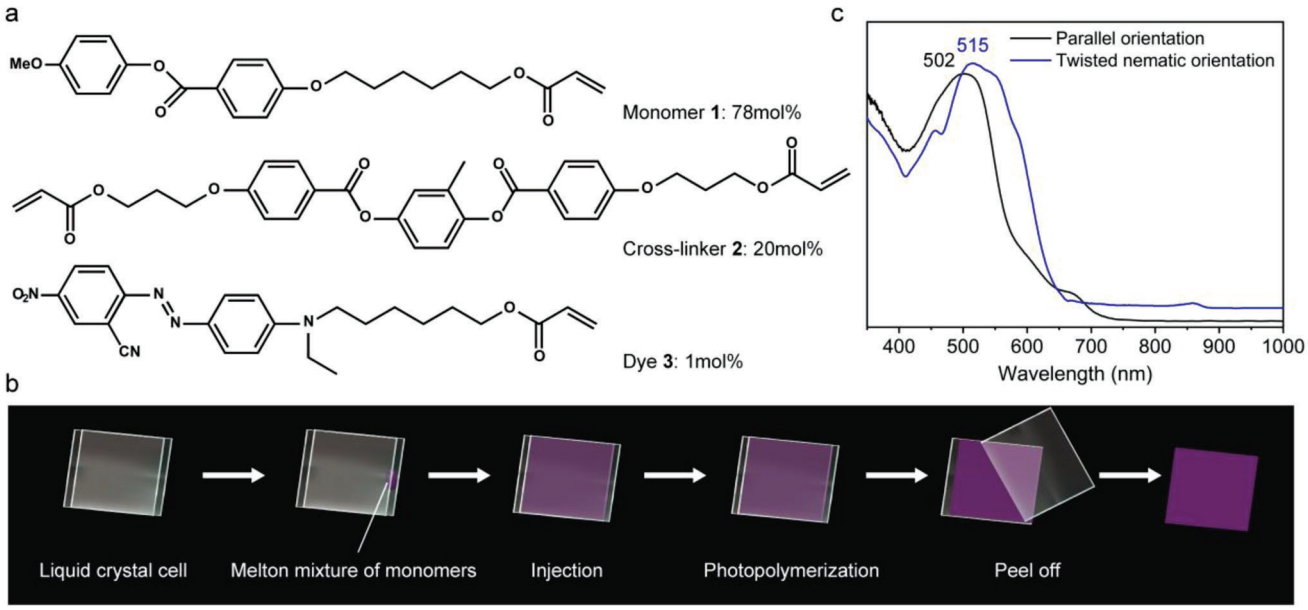

Figure 1. a) Chemical structures and molar ratio of LC monomer mixtures for preparation of CLCP films. 1: LC monomer, 2: LC cross-linker, 3: dye. b) Schematic illustration of one-step method for preparation of CLCP films. c) Absorption spectra of synthesized parallel and twisted nematic orientation CLCP films.

2.3. CLCP Micromirror Preparation

The fabrication process for CLCP micromirror is shown in Figure S2a (Supporting Information). First, a steel foil mask with a thickness of 10 μm was generated using femtosecond laser micromachining.[43] Then the mask was fixed onto the CLCP film and put into a high vacuum evaporation coating system to form the micromirror reflection layer (Cr (5 nm)/Au (150 nm)). Finally, the CLCP micromirror was formed by femtosecond laser direct writing of CLCP film along the mirror surface edge. The optical image of the fabricated CLCP micromirror is shown in Figure S2b (Supporting Information). The reflection surface size of the micromirror was 1400 μm × 1400 μm, and the size of the driving beam was 1600 μm × 450 μm. The reflection spectrum of the mirror surface is shown in Figure S2c (Supporting Information), indicating a good reflectance capacity.

2.4. CLCP Microstructure Actuation

Figure S3 (Supporting Information) shows the experimental setup for driving the CLCP microstructure. An ultrafast fiber amplifier system (Amplitude) delivering a central wavelength of 1030 nm, pulse duration of 130 fs, and beam diameter of 3 mm (at e^{-2}) was used as the initial light source. Then a BBO crystal was employed to tune the laser wavelength to 515 nm to match the absorption of the CLCP films. After that, the laser beam diameter was expanded to 12 mm by a beam expander and incident to spatial light modulator (SLM). After phase modulation by the SLM, the laser beam was focused onto the driving beam of CLCP microstructure via a convex lens with focal length of $f = 150$ mm. Upon irradiation of 515 nm light and reaching a certain light intensity, the driving beam of the CLCP microstructure would be bent or twisted, causing deflection of mirror surface, thereby changing the light reflection direction that was incident to the mirror surface. Two CCD cameras were utilized to observe the light pattern irradiation position and light-driven behaviors of CLCP microstructures from the front and side view, respectively.

3. Results and Discussion

3.1. Machining Parameter Optimization

Figure 2a shows comparisons of machining speed and resolution for femtosecond laser with those of clipping,[53–57] 3D printing[58–61] and two-photon polymerization,[62–65] indicating that FsLDW can provide both a quick machining speed and high resolution. Figure 2b demonstrates that FsLDW method can achieve various pattern micromachining. For CLCP film micromachining, the microstructure edge HAZ is a main influence factor on the minimum machining size, as when the structure size is determined, a larger HAZ will result in a smaller effective size. It is only when the efficient size of CLCP microstructure reaches a certain value, the microstructure can be driven. Here, the microstructure HAZ was measured or estimated using a confocal laser scanning microscope (Carl Zeiss, LSM 900), because after laser thermal ablation, the microstructure edge presents a darker color band due to carbonization (Figure S4, Supporting Information). Moreover, we have quantified the HAZ using a polarizing microscope (Leica, DM2700P, Germany). As shown in Figure S5 (Supporting Information), the birefringence of liquid crystal materials (light and dark field change) is hard to observe in the microstructure edge, indicating that the HAZ shows a different optical property compared to that unprocessed area. The

© 2023 Wiley-VCH GmbH

2365709x, 0, Downloaded from https://onlinelibrary.wiley.com/doi/10.1002/admt.202300967 by Zhejiang University, Wiley Online Library on [04/10/2023]. See the Terms and Conditions (https://onlinelibrary.wiley.com/terms-and-conditions) on Wiley Online Library for rules of use; OA articles are governed by the applicable Creative Commons License

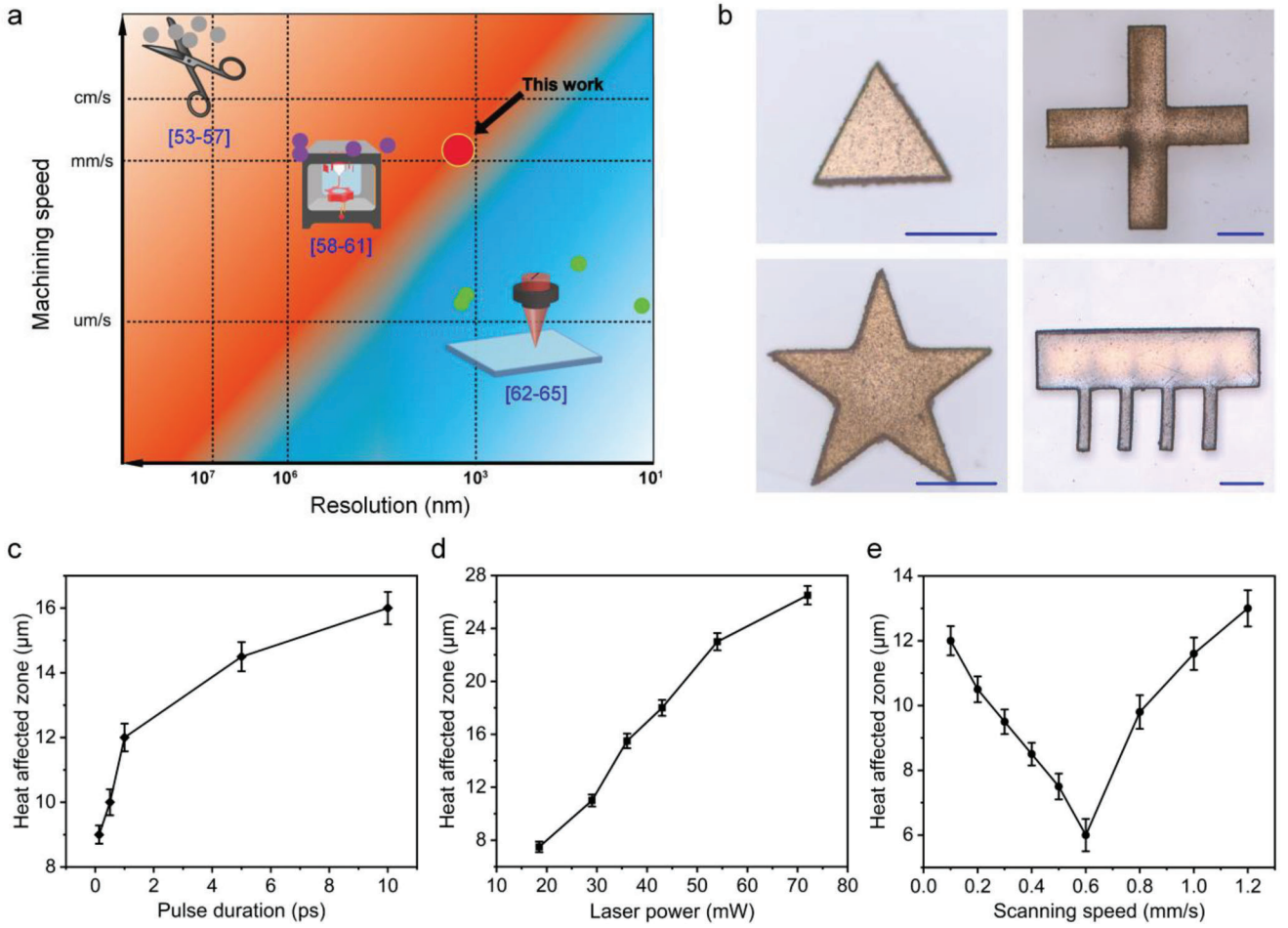

Figure 2. a) Comparisons of machining speed and resolution for this work with traditional clipping, 3D printing, and two-photon polymerization. b) Optical images of prepared various shape CLCP microstructures. All scale bars are 200 μm. c) CLCP microstructure HAZ as a function of laser pulse duration. The laser repetition rate is 0.8 kHz (power of 30 mW) and the pulse duration is varied from 130 fs to 10 ps. d) CLCP microstructure HAZ under different laser machining powers. The laser pulse duration is 130 fs and the repetition rate is varied from 0.5 to 2 kHz (laser powers varying from 19 to 70 mW). e) CLCP microstructure HAZ as a function of laser scanning speed. The laser pulse duration is 130 fs with a repetition rate of 0.8 kHz (power of 30 mW) and the laser scanning speed is varied from 0.2 to 1.2 mm^{-1} s.

measured HAZ using a polarizing microscope is consistent with that using a confocal laser scanning microscope.

To reduce microstructure HAZ, we further optimized machining parameters. Figure 2c shows CLCP microstructure HAZ changes under different laser pulse durations. As the laser pulse duration decreases or pulse peak energy increases, the microstructure HAZ can be significantly reduced, as shown in Figure S6 (Supporting Information). The laser power effect on CLCP microstructure HAZ was also investigated, with results shown in Figure 2d. As the laser power is increased, the microstructure HAZ is increased, as illustrated in Figure S7 (Supporting Information). Therefore, the laser power should be controlled in a reasonable range during the processing. On the one hand, it should enable cutting through the CLCP film, on the other hand, it should not be too high to reduce the thermal ablation. Figure 2e shows CLCP microstructure HAZ changes under different scanning speeds. As the laser scanning speed is increased from 0.2 to 0.6 mm^{-1} s, the CLCP microstructure HAZ is decreased. It is mainly due to that when the laser power is slightly larger than the ablation threshold of the CLCP film, a relatively quick scanning speed can reduce the thermal ablation time, thus decreasing the HAZ. Whereas, as the scanning speed is further increased to 1.2 mm^{-1} s, the microstructure HAZ is increased, mainly due to that over-quick machining speed results in an insufficient cutting of the CLCP film and causing the edge burr, as shown in Figure S8 (Supporting Information). In addition, it should be noted that although the cutting/scanning speed of ≈0.6 mm^{-1} s can provide a relatively smaller HAZ, the processed microstructure edge is not smooth and has a certain edge burr. Therefore, we identify the optimum processing parameters of laser pulse duration of 130 fs, power of 20–25 mW, and cutting speed of 0.3–0.4 mm^{-1} s, which can reach a minimum machining size of 40 μm and an average HAZ smaller than 8 μm. We have also investigated different sample HAZs at the same machining parameters. The results show that for different samples with the same thickness, they can achieve

© 2023 Wiley-VCH GmbH

2365709x, 0, Downloaded from https://onlinelibrary.wiley.com/doi/10.1002/admt.202300967 by Zhejiang University, Wiley Online Library on [04/10/2023]. See the Terms and Conditions (https://onlinelibrary.wiley.com/terms-and-conditions) on Wiley Online Library for rules of use; OA articles are governed by the applicable Creative Commons License

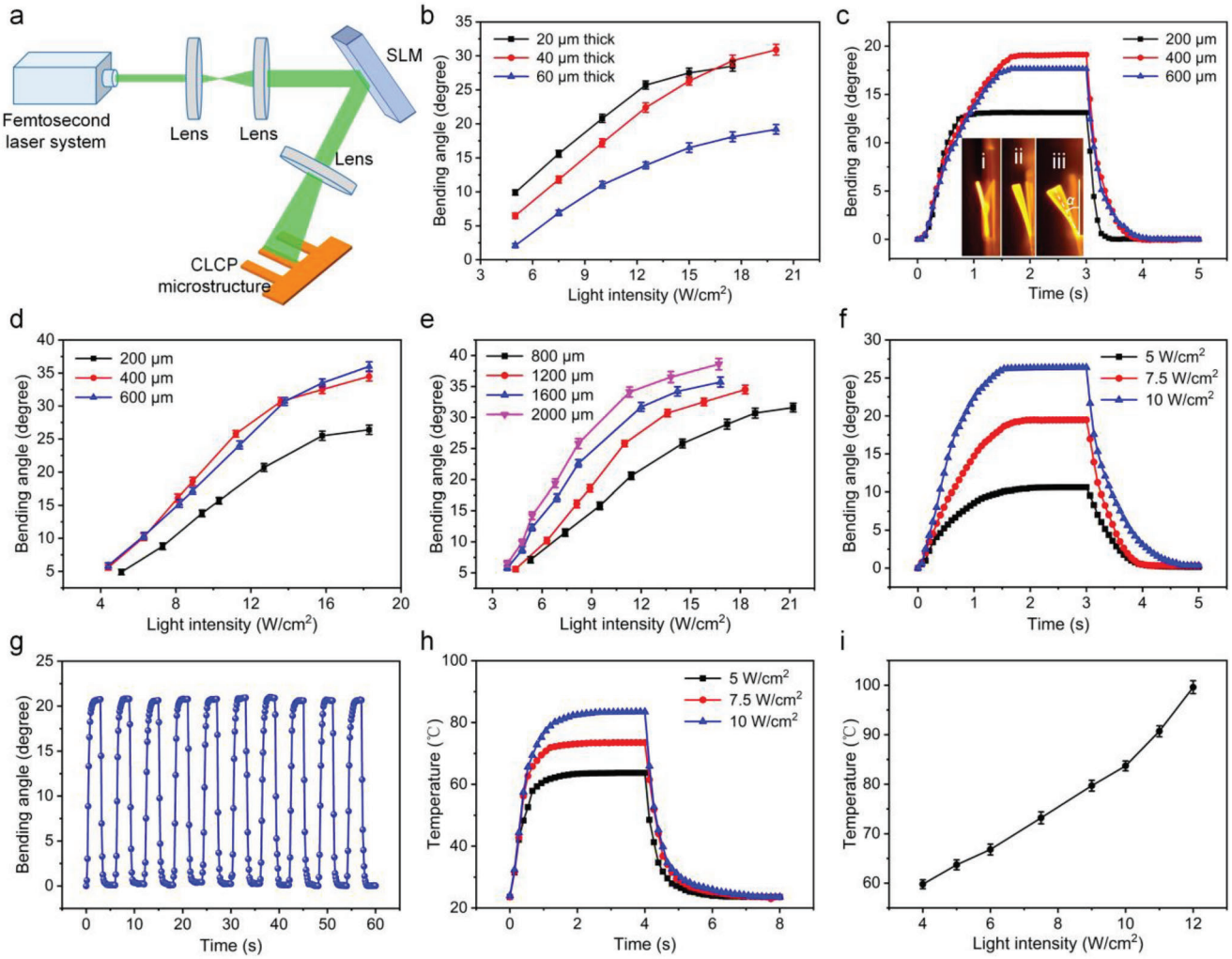

Figure 3. a) Simplified schematic of experimental setup for driving the CLCP cantilever. b) Comparisons of bending angles for CLCP cantilevers with different thicknesses (20 to 60 μm) under different light intensities. The cantilever size is 1200 μm × 400 μm. c) Bending angles as a function of light irradiation time for CLCP cantilevers with a length of 1200 μm and varied widths of 200 to 600 μm. The light irradiation time is 3s with a light intensity of 9 W cm^{-2}. The inset shows bending behaviors of CLCP cantilevers with widths of i) 200 μm, ii) 400 μm iii) 600 μm. d) Bending angles for CLCP cantilevers with a length of 1200 μm and varying widths of 200 to 600 μm under different light intensities. The light irradiation time is 3 s. e) Bending angles for CLCP cantilevers with width of 400 μm and varied lengths of 800 to 2000 μm under different light intensities. The light irradiation time is 3 s. f) Bending angles as a function of light irradiation time for CLCP cantilevers under different light intensities. The cantilever size is 1600 μm × 400 μm, and the light irradiation time is 3 s. g) The stability and repeatability of the bending for CLCP cantilever at the same light intensity cycle. The cantilever size is 1600 μm × 400 μm and the light irradiation time is open 2s and closed 3s. The light intensity is 8 W cm^{-2}. h) Cantilever temperature as a function of light irradiation time under different light intensities. The cantilever size is 1600 μm × 400 μm and the light irradiation time is 3 s. i) Cantilever heating temperatures under different light intensities. The light irradiation time is 3 s.

a stable HAZ ≈7–8 μm, as shown in Figure S9 (Supporting Information), indicating that the proposed method has good reproducibility from sample to sample.

3.2. CLCP Microstructure Light-Responsive Characterization

Based on the above micromachining system, we prepared different length-width ratio cantilevers and characterized their light-driven behaviors. We first investigated light-responsive behaviors of parallel nematic orientation CLCP cantilevers. During the cutting process, the length direction of the cantilever is along the orientation of mesogen molecular and the simplified schematic of experimental setup for driving the CLCP cantilever can refer to **Figure 3**a. During the driving process, the light spot generated by the SLM is a rectangle pattern with a size slightly larger than the CLCP cantilever. The bending angle of the cantilever is defined as the included angle between CLCP component surface and the central axis of cantilever and was measured or estimated according to optical images.

Figure 3b shows the bending angles of CLCP cantilevers with different film thicknesses (20 to 60 μm) under different light intensities. The bending angle of the cantilever is increased with the increase of light intensity. The 60 μm-thick CLCP cantilever

© 2023 Wiley-VCH GmbH

2365709x, 0, Downloaded from https://onlinelibrary.wiley.com/doi/10.1002/admt.202300967 by Zhejiang University, Wiley Online Library on [04/10/2023]. See the Terms and Conditions (https://onlinelibrary.wiley.com/terms-and-conditions) on Wiley Online Library for rules of use; OA articles are governed by the applicable Creative Commons License

presents a smaller bending angle than those of 20 μm-thick and 40 μm-thick ones at the same light intensity, probably due to the increase of film thickness improves the rigidity of the cantilever. Another reason may be that when the light penetration depth is constant, a thicker film results in a smaller penetration ratio (light penetration length divided by the film thickness). For 20 μm-thick CLCP cantilever, there is a threshold light intensity (≈12.5 W cm^{-2}), above which, the cantilever is hard to produce a reversible deformation. This is the reason that when the light intensity exceeds 12.5 W cm^{-2}, the increased trend of bending angles with the light intensity slows down. In addition, there is a light intensity threshold to totally damage the structure. For 20 μm-thick CLCP cantilever, it presents a lower value ≈18 W cm^{-2}. Therefore, in consideration of CLCP microstructure strength, damage threshold, and bending performance, all the thickness of the CLCP film is 40 μm for the following experiments.

Then we further studied effects of cantilever length-width ratio on bending behaviors. In order to make results comparable, the prepared microstructure in Figures 3c–g is from the same CLCP film and fabricated under identical conditions. Figure 3c shows bending angles as a function of light irradiation time for CLCP cantilevers with a length of 1200 μm and widths varying from 200 to 600 μm. Upon irradiation of 515 nm light, the CLCP cantilever is rapidly bended. With the duration of light irradiation, the bending angle tends to be steady at a constant value. The bending speeds for different-width cantilevers are nearly the same at the same light intensity. However, the 200 μm-width cantilever can quickly reach a relatively stable state (≈1 s) due to its smaller bending angle. In addition, as the cantilever width increases, the cantilever tends to produce a lateral torsion except for an out-of-plane bending, as shown in the inset of Figure 3c. The measured width threshold for generating a distinct lateral torsion is ≈450–500 μm, which is probably due to a non-uniform light density generated by the SLM or poor structural stability caused by a thinner film. Figure 3d summarizes bending angles for different-width cantilevers under different light intensities. For all the width cantilevers, the bending angles are increased with the light intensity. The 200 μm-width cantilever shows a smaller bending angle than those of 400 μm-width and 600 μm-width ones. Besides, the 600 μm-width cantilever tends to have a distinct lateral torsion (see inset in Figure 3c). Therefore, the width of 400 μm is chosen to further analyze the length effects for the following experiments.

Figure 3e compares bending angles for different-length cantilevers under different light intensities. Clearly, the bending angle of the cantilever is increased with the increase of cantilever length or light intensity. However, when the light intensity reaches a certain value, there is no prominent increase in bending angle with the light intensity, otherwise, the cantilever will be damaged. In addition, the bending speed of the cantilever is increased with the light intensity, as shown in Figure 3f. The response time of the cantilever is ≈2 s (from beginning the bending to reaching a relatively constant bending state). Figure 3g demonstrates that the bending of the CLCP cantilever driven by the light can achieve good stability and repeatability.

We have also measured temperature changes of CLCP cantilever as a function of light irradiation time under different light intensities using an infrared thermometer (A665sc, FLIR). As shown in Figure 3h, upon irradiation of 515 nm light, the temperature of cantilever is quickly gone up. With the duration of light irradiation, the cantilever temperature will reach a relatively stable state due to the thermal equilibrium between light irradiation heating and heat dissipation from the surrounding air. As the light intensity increases, the temperature rising rate of the cantilever is improved, and the final heating temperature is also increased, as shown in Figure 3i. Moreover, the temperature rising time and the bending time of the cantilever upon irradiation of 515 nm light are nearly the same (≈2 s), indicating that the bending of the cantilever is mainly due to the temperature change or thermal phase transition.

To achieve more complex motion, a twisted nematic (TN) liquid crystal cell was used to prepare the CLCP film with twisted nematic geometry, as shown in **Figure 4**a. In a twisted nematic liquid crystal cell, the liquid crystal molecules experience a twist as they move from one substrate to another. The twist is achieved by introducing a 90° phase difference between two alignment directions.[66] As a result, the liquid crystal molecules rotate by 90 degrees over the thickness of the cell. Then the samples were cut in different directions, here a cutting angle (θ) between the orientation of the molecules at mid-plane and the cutting direction was defined. When the cutting angle is 45° or 135°, the formed cantilever is twisted in the clockwise direction or counterclockwise direction, respectively, upon irradiation of 515 nm light, as shown in Figure 4b, Movies S1 and S2 (Supporting Information). As the light intensity is increased, the twisting angle is increased, as illustrated in Figure 4c. There is a threshold light intensity (≈10 W cm^{-2}), above which, the cantilever will be easy to damage or fracture. Then we further investigated the effects of light irradiation location on twisting behaviors of the cantilever. As shown in Figure 4d, the twisting position of the cantilever can be adjusted by the light irradiation location, and only the location irradiated by the light can generate a twisting deformation. The closer the light irradiation location near the cantilever root, the larger the twisting deformation. In addition, as shown in Figure 4e,f, no apparent gravity effect on twisting behaviors of the cantilever was observed, while the increase of light intensity could make the cantilever twisting angle >450°, as depicted in Figure S10 (Supporting Information).

When the cutting angle is 90°, the cantilever will present an out-of-plane bending upon irradiation of 515 nm light, and no obvious twisting behavior was observed, as shown in Figure 4g and Movie S3 (Supporting Information). Figure 4h shows bending angles of the cantilever as a function of light irradiation time at a light intensity of 2.5 W cm^{-2}. Upon irradiation of 515 nm light, the bending angle of the cantilever is rapidly increased. With the duration of light irradiation, the bending angles tend to reach a constant value. When the driven light is closed, the bent cantilever will gradually return to its initial state. Figure 4i summarizes bending angles of the cantilever under different light intensities. The measured reversible maximum bending angle is ≈38°, above which, the cantilever is difficult to recover to its initial state. We have also observed that twisting or bending behaviors of the cantilever are not sensitive to the light polarization but sensitive to the light incident angle, as shown in Figure S11 (Supporting Information).

© 2023 Wiley-VCH GmbH

2365709x, 0, Downloaded from https://onlinelibrary.wiley.com/doi/10.1002/admt.202300967 by Zhejiang University, Wiley Online Library on [04/10/2023]. See the Terms and Conditions (https://onlinelibrary.wiley.com/terms-and-conditions) on Wiley Online Library for rules of use; OA articles are governed by the applicable Creative Commons License

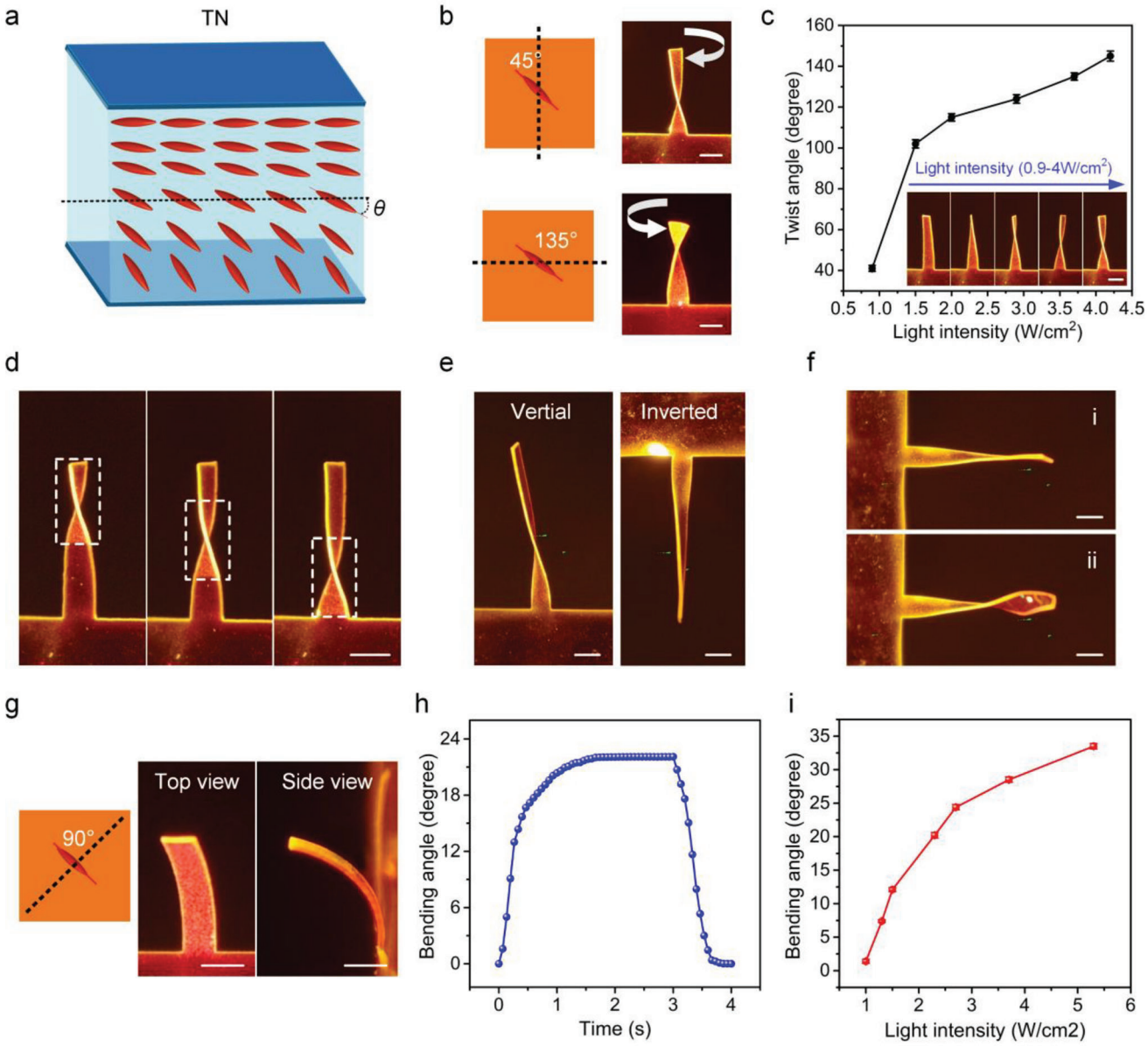

Figure 4. a) Schematic showing twisted nematic geometry of mesogens in CLCP film. b) Twisting behaviors of the CLCP cantilever when the cutting angle is 45° and 135°, respectively. c) Twisting angles of the cantilever under different light intensities when the cutting angle is 45°. The insets show twisting angle changes with the increase of light intensity. d) Twisting behaviors of the cantilever at different light irradiation locations. The light spot length is equal to half the length of the cantilever, and the width is slightly larger than the cantilever width. The area of the white dotted line represents the light irradiation location. e) Twisting behaviors of the cantilever in vertical and inverted placed directions. f) Twisting behaviors of the cantilever at lateral placed direction, for i with a light intensity of 2 W cm^{-2} and ii with a light intensity of 4 W cm^{-2}. g) Bending behaviors of the cantilever when the cutting angle is 90°. h) Bending angles of the cantilever as a function of light irradiation time when the cutting angle is 90°. The light irradiation time is 3s with a light intensity of 2.5 W cm^{-2}. i) Bending angles of the cantilever under different light intensities when the cutting angle is 90°. The light irradiation time is 3s. All scale bars are 500 μm.

3.3. Demonstration of Light-Driven CLCP Micromirror

To demonstrate the applications of CLCP microstructures, we propose a light-driven CLCP micromirror system. The fabrication process of CLCP micromirror has been described in detail in Experimental Section. The CLCP micromirror consists of a driving beam and a reflection mirror surface. During the test, a 515 nm rectangle light pattern generated by the SLM is irradiated on the driving beam of the CLCP micromirror. Upon radiation of 515 nm light, the driven beam will be bent or twisted, and then causing the deflection of mirror surface. If a light beam is irradiated on the mirror surface, the light propagation direction or path will be modulated, as depicted in **Figure 5**a.

As demonstrated above, the bending or twisting motion can be achieved using the parallel orientation or twisted nematic orientation CLCP cantilevers. Here, we demonstrate a swing

© 2023 Wiley-VCH GmbH

2365709x, 0, Downloaded from https://onlinelibrary.wiley.com/doi/10.1002/admt.202300967 by Zhejiang University, Wiley Online Library on [04/10/2023]. See the Terms and Conditions (https://onlinelibrary.wiley.com/terms-and-conditions) on Wiley Online Library for rules of use; OA articles are governed by the applicable Creative Commons License

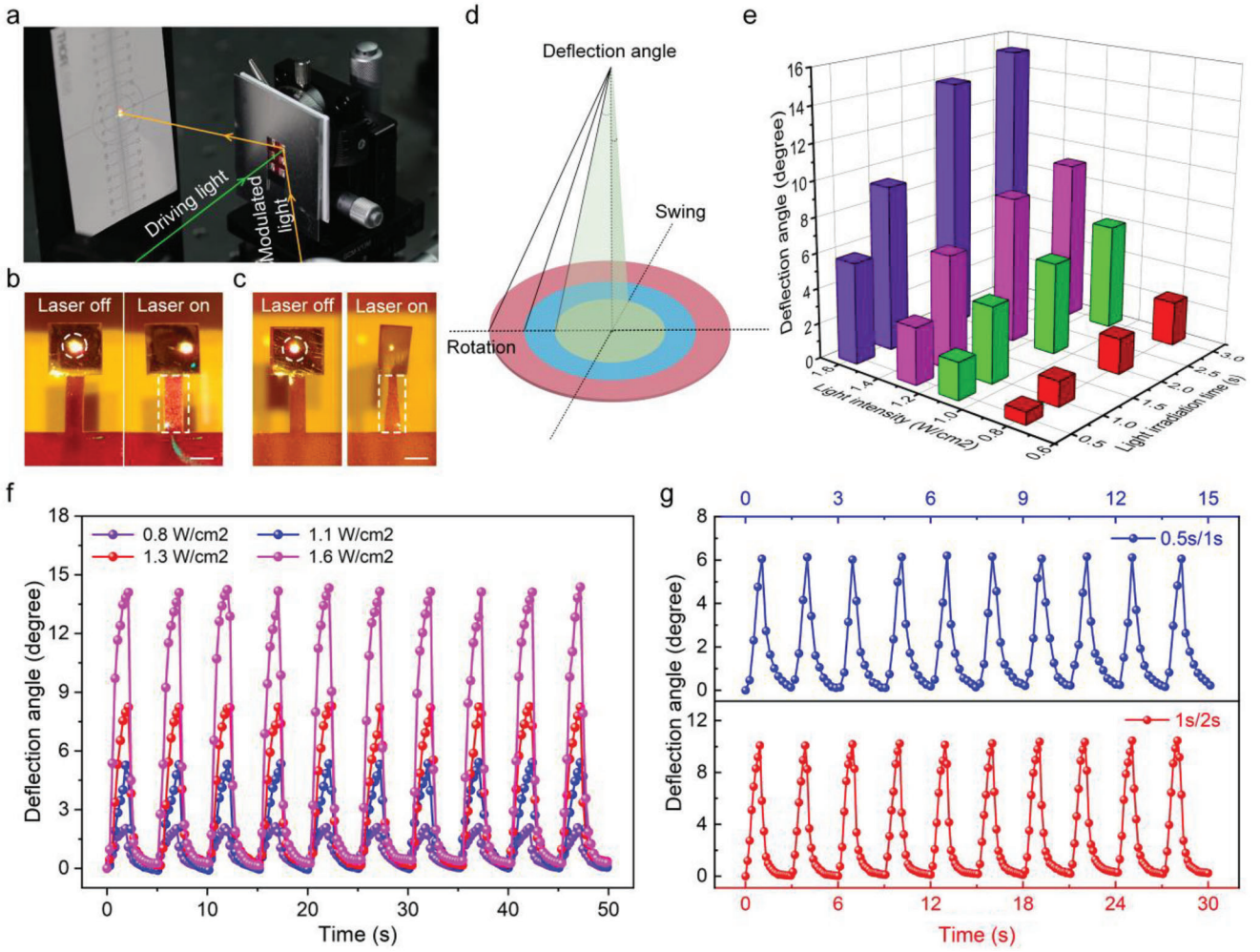

Figure 5. a) Partial image of the experiment setup for the light-driven micromirror system. In test, the driven light generated by the SLM is irradiated on the driving beam, and the modulated light is irradiated on the reflection mirror surface. A card is used to receive the reflected light for analyzing the deflection angle of the modulated light. b) Optical image of the swing of the CLCP micromirror. The driving beam of the micromirror is bended upon irradiation of 515 nm light. The rectangular dotted area represents the light irradiation location, and the circular dotted area represents the modulated light spot location. c) Optical image of rotation motion of the CLCP micromirror. The driving beam of the micromirror is twisted upon irradiation of 515 nm light. d) Schematic diagram of light spot movement on the card under swing or rotation of the mirror surface. e) Deflection angles (average value) of the modulated light under different light intensities and light irradiation time. f) Deflection angles of the modulated light as a function of light irradiation time under different light intensity cycles. The driven light is open 2 s and closed 3 s. g) Deflection angles of the modulated light as a function of light irradiation time under different light irradiation periods. All scale bars are 500 μm.

or rotation motion of the mirror surface using the proposed micromirror system. For example, if the micromirror is based on parallel orientation CLCP film, the swing of the mirror surface can be easily realized upon radiation of 515 nm light, as shown in Figure 5b and Movie S4 (Supporting Information). If the micromirror is based on twisted nematic geometry CLCP film, the swing and rotation motion of the mirror surface can be achieved simultaneously using the micromirror system by cutting the driving beam in different directions, as shown in Figures 5c and Movie S5 (Supporting Information). Figure 5d shows the schematic of light spot movement path under swing or rotation motion of the mirror surface. The deflection angle can be calculated by the distance of the light spot moved. Figure 5e shows the deflection angle of the modulated light under different light intensities and light irradiation time. As the light intensity or light irradiation time is increased, the deflection angle is increased. Figure 5f demonstrates the deflection angle of the modulated light can be controlled by the light intensity and shows good repeatability under different light intensities (Movies S6 and S7, Supporting Information). Moreover, the deflection angle of the modulated light can be controlled by the light irradiation time when the light intensity is fixed, as shown in Figure 5g, Movies S8 and S9 (Supporting Information). In addition, the proposed CLCP micromirror system shows good stability, as shown in Figure S12 (Supporting Information). The maximum scanning frequency of the micromirror is ≈2 Hz (Movies S10 and S11, Supporting Information). Therefore, the proposed light-driven micromirror system can not only achieve the modulation of light reflection direction but also control the light deflection angle through light intensity and irradiation time, showing great

© 2023 Wiley-VCH GmbH

2365709x, 0, Downloaded from https://onlinelibrary.wiley.com/doi/10.1002/admt.202300967 by Zhejiang University, Wiley Online Library on [04/10/2023]. See the Terms and Conditions (https://onlinelibrary.wiley.com/terms-and-conditions) on Wiley Online Library for rules of use; OA articles are governed by the applicable Creative Commons License

potential for applications in optical trigger switches and lidar systems. In addition, as the CLCP micromirror is driven by light, it avoids the effect of electromagnetic interference.

4. Conclusion

In summary, a femtosecond laser direct writing method has been proposed for CLCP microstructure construction and light-driven CLCP micromirror preparation. Through systematic investigation of effects of laser pulse duration, power, and scanning speed on CLCP microstructure HAZ, the optimized machining parameters of laser pulse duration of 130 fs, power of 20–25 mW, and scanning speed of ≈0.4 mm^{-1} s are determined, which enables arbitrary pattern micromachining with a minimum size of 40 μm and an average HAZ smaller than 8 μm. Then, we further investigated their light-responsive behaviors and analyzed the effects of the structure length-width ratio, cutting direction, light irradiation time, incident angle, and light intensity on bending and twisting behaviors, providing a guide for optimum design and actuation of CLCP microstructure. Finally, we demonstrate a controllable light-driven CLCP micromirror system, which can achieve not only a swing but also a rotation of the mirror surface with a maximum scanning frequency of ≈2 Hz. Our work shows great potential for construction of light-driven CLCP microactuators using laser micromachining for applications in optical trigger switches, lidar, and soft actuators.

Supporting Information

Supporting Information is available from the Wiley Online Library or from the author.

Acknowledgements

This work was supported by the National Natural Science Foundation of China (61927820, 12004314, 62105269). The authors thank the technical support from Center for Micro/Nano Fabrication and Instrumentation and the Service Center for Molecular Sciences at Westlake University. The authors thank Ms. Danyu Gu for measuring the absorption spectra and Dr. Lei Zhang for the evaporation of Au film.

Conflict of Interest

The authors declare no conflict of interest.

Author Contributions

Y.W. and Y.L. contributed equally to this paper. M.Q. and J.A.L. supervised the whole project. M.Q. and J.A.L. conceived the experiments. Y.W., J.G., and Y.L. constructed the experimental setup. Y.W. and Y.L. carried out the experiments. Y.W. and Y.L. wrote the manuscript. All authors participated in the revision of the manuscript.

Data Availability Statement

The data that support the findings of this study are available in the supplementary material of this article.

Keywords

controllable shape morphing, femtosecond laser direct writing, light-driven micromirrors, liquid crystal polymers, microactuators

Received: June 14, 2023
Revised: August 27, 2023
Published online:

[1] M. Pilz Da Cunha, M. G. Debije, A. P. H. J. Schenning, *Chem. Soc. Rev.* **2020**, *49*, 6568.
[2] M. R. A. Bhatti, E. Bilotti, H. Zhang, S. Varghese, R. C. P. Verpaalen, A. P. H. J. Schenning, C. W. M. Bastiaansen, T. Peijs, *ACS Appl. Mater. Interfaces* **2020**, *12*, 33210.
[3] Y. Takashima, S. Hatanaka, M. Otsubo, M. Nakahata, T. Kakuta, A. Hashidzume, H. Yamaguchi, A. Harada, *Nat. Commun.* **2012**, *3*, 1270.
[4] F. Siebers, A. Jayaram, P. Blümler, T. Speck, *Sci. Adv.* **2023**, *9*, eadf5443.
[5] X.-Q. Wang, K. H. Chan, Y. Cheng, T. Ding, T. Li, S. Achavananthadith, S. Ahmet, J. S. Ho, G. W. Ho, *Adv. Mater.* **2020**, *32*, 2000351.
[6] R. Wang, L. Han, C. Wu, Y. Dong, X. Zhao, *ACS Appl. Mater. Interfaces* **2022**, *14*, 6138.
[7] Y. Xiang, B. Li, B. Li, L. Bao, W. Sheng, Y. Ma, S. Ma, B. Yu, F. Zhou, *ACS Appl. Mater. Interfaces* **2022**, *14*, 20291.
[8] O. M. Wani, H. Zeng, A. Priimagi, *Nat. Commun.* **2017**, *8*, 15546.
[9] D. Jiang, S.-Y. Park, *Lab Chip* **2016**, *16*, 1831.
[10] J.-A. Lv, Y. Liu, J. Wei, E. Chen, L. Qin, Y. Yu, *Nature* **2016**, *537*, 179.
[11] Y. Hu, Q. Ji, M. Huang, L. Chang, C. Zhang, G. Wu, B. Zi, N. Bao, W. Chen, Y. Wu, *Angew. Chem., Int. Ed.* **2021**, *60*, 20511.
[12] Z. Hu, Y. Li, J.-A. Lv, *Nat. Commun.* **2021**, *12*, 3211.
[13] J. Sun, W. Hu, L. Zhang, R. Lan, H. Yang, D.-K. Yang, *Adv. Funct. Mater.* **2021**, *31*, 2103311.
[14] T. J. White, D. J. Broer, *Nature Mater* **2015**, *14*, 1087.
[15] J. Jiang, L.i Han, F. Ge, Y. Xiao, R. Cheng, X. Tong, Y. Zhao, *Angew. Chem., Int. Ed.* **2022**, *134*, 202116689.
[16] Y. Li, Y. Liu, D. Luo, *Adv. Optical Mater.* **2021**, *9*, 2001861.
[17] J. Hu, Z. Nie, M. Wang, Z. Liu, S. Huang, H. Yang, *Angew. Chem., Int. Ed.* **2023**, *62*, 202218227.
[18] J. Hu, M. Yu, M. Wang, K.-L. Choy, H. Yu, *ACS Appl. Mater. Interfaces* **2022**, *14*, 12951.
[19] Y. Shang, J. Wang, T. Ikeda, L. Jiang, *J. Mater. Chem. C* **2019**, *7*, 3413.
[20] T. J. White, *J. Polym. Sci., Part B: Polym. Phys.* **2018**, *56*, 695.
[21] X. Qing, L. Qin, W. Gu, Y. Yu, *Liq. Cryst.* **2016**, *43*, 2114.
[22] T. Ube, K. Kawasaki, T. Ikeda, *Adv. Mater.* **2016**, *28*, 8212.
[23] C. Zhu, Y. Lu, J. Sun, Y. Yu, *Langmuir* **2020**, *36*, 6611.
[24] L. Qin, X. Liu, Y. Yu, *Adv. Optical Mater.* **2021**, *9*, 2001743.
[25] G. Stoychev, A. Kirillova, L. Ionov, *Adv. Optical Mater.* **2019**, *7*, 1900067.
[26] X. Pang, J.-A. Lv, C. Zhu, L. Qin, Y. Yu, *Adv. Mater.* **2019**, *31*, 1904224.
[27] F. Cheng, R. Yin, Y. Zhang, C.-C. Yen, Y. Yu, *Soft Matter* **2010**, *6*, 3447.
[28] S. Chen, Y. Cao, M. Sarparast, H. Yuan, L. Dong, X. Tan, C. Cao, *Adv. Materi. Technol.* **2020**, *5*, 1900837.
[29] B. Zuo, M. Wang, B.-P. Lin, H. Yang, *Nat. Commun.* **2019**, *10*, 4539.
[30] C. L. Van Oosten, C. W. M. Bastiaansen, D. J. Broer, *Nature Mater* **2009**, *8*, 677.
[31] Y. Liu, W. Wu, J. Wei, Y. Yu, *ACS Appl. Mater. Interfaces* **2017**, *9*, 782.
[32] J. M. Mccracken, B. R. Donovan, K. M. Lynch, T. J. White, *Adv. Funct. Mater.* **2021**, *31*, 2100564.
[33] Y. Liu, B. Xu, S. Sun, J. Wei, L. Wu, Y. Yu, *Adv. Mater.* **2017**, *29*, 1604792.
[34] X.-Q. Wang, G. W. Ho, *Mater. Today* **2022**, *53*, 197.
[35] J.-A. Lv, W. Wang, W. Wu, Y. Yu, *J. Mater. Chem. C* **2015**, *3*, 6621.

© 2023 Wiley-VCH GmbH

2365709x, 0, Downloaded from https://onlinelibrary.wiley.com/doi/10.1002/admt.202300967 by Zhejiang University, Wiley Online Library on [04/10/2023]. See the Terms and Conditions (https://onlinelibrary.wiley.com/terms-and-conditions) on Wiley Online Library for rules of use; OA articles are governed by the applicable Creative Commons License

[36] C. P. Ambulo, J. J. Burroughs, J. M. Boothby, H. Kim, M. R. Shankar, T. H. Ware, *ACS Appl. Mater. Interfaces* **2017**, *9*, 37332.
[37] S. Gantenbein, K. Masania, W. Woigk, J. P. W. Sesseg, T. A. Tervoort, A. R. Studart, *Nature* **2018**, *561*, 226.
[38] F. Ge, Y. Zhao, *Adv. Funct. Mater.* **2020**, *30*, 1901890.
[39] Z. Wang, Y. Guo, S. Cai, J. Yang, *ACS Appl. Polym. Mater.* **2022**, *4*, 3153.
[40] Y. Shi, P. S. Salter, M. Li, R. A. Taylor, S. J. Elston, S. M. Morris, D. D. C. Bradley, *Adv. Funct. Mater.* **2021**, *31*, 2007493.
[41] Y. Guo, H. Shahsavan, M. Sitti, *Adv. Optical Mater.* **2020**, *8*, 1902098.
[42] L. Li, W. Kong, F. Chen, *Adv. Photonics* **2022**, *4*, 024002.
[43] Y. Wang, J. Qian, *ACS Omega* **2023**, *8*, 7838.
[44] B.-B. Xu, Y.-L. Zhang, H. Xia, W.-F. Dong, H. Ding, H.-B. Sun, *Lab Chip* **2013**, *13*, 1677.
[45] G.-L. Roth, C. Esen, R. Hellmann, *Opt. Express* **2017**, *25*, 18442.
[46] T. Grossmann, S. Schleede, M. Hauser, T. Beck, M. Thiel, G. Von Freymann, T. Mappes, H. Kalt, *Opt. Express* **2011**, *19*, 11451.
[47] Y.-L. Zhang, Q.-D. Chen, H. Xia, H.-B. Sun, *Nano Today* **2010**, *5*, 435.
[48] R. Li, D. Jin, D. Pan, S. Ji, C. Xin, G. Liu, S. Fan, H. Wu, J. Li, Y. Hu, D. Wu, L. Zhang, J. Chu, *ACS Nano* **2020**, *14*, 5233.
[49] Y.-L. Sun, W.-F. Dong, L.-G. Niu, T. Jiang, D.-X. Liu, L. Zhang, Y.-S. Wang, Q.-D. Chen, D.-P. Kim, H.-B. Sun, *Light.: Sci. Appl.* **2014**, *3*, 129.
[50] Z.-C. Ma, Y.-L. Zhang, B. Han, Q.-D. Chen, H.-B. Sun, *Small Methods* **2018**, *2*, 1700413.
[51] Z. Y. Hu, Y. L. Zhang, C. Pan, J. Y. Dou, Z. Z. Li, Z. N. Tian, J. W. Mao, Q. D. Chen, H. B. Sun, *Nat. Commun.* **2022**, *13*, 5634.
[52] D. J. Broer, H. Finkelmann, K. Kondo, *Die Makromol. Chem.* **1988**, *189*, 185.
[53] X. Yang, Y. Chen, X. Zhang, P. Xue, P. Lv, Y. Yang, L. Wang, W. Feng, *Nano Today* **2022**, *43*, 101419.
[54] C. Shen, R. Lan, R. Huang, Z. Zhang, J. Bao, L. Zhang, H. Yang, *ACS Appl. Mater. Interfaces* **2021**, *13*, 3221.
[55] H. Zeng, O. M. Wani, P. Wasylczyk, R. Kaczmarek, A. Priimagi, *Adv. Mater.* **2017**, *29*, 1701814.
[56] M. Pilz Da Cunha, S. Ambergen, M. G. Debije, E. F. G. A. Homburg, J. M. J. Den Toonder, A. P. H. J. Schenning, *Adv. Sci.* **2020**, *7*, 1902842.
[57] S. Iamsaard, E. Anger, S. J. Aßhoff, A. Depauw, S. P. Fletcher, N. Katsonis, *Angew. Chem., Int. Ed.* **2016**, *128*, 10062.
[58] M. Barnes, S. M. Sajadi, S. Parekh, M. M. Rahman, P. M. Ajayan, R. Verduzco, *ACS Appl. Mater. Interfaces* **2020**, *12*, 28692.
[59] Y. Wang, R. Yin, L. Jin, M. Liu, Y. Gao, J. Raney, S. Yang, *Adv. Funct. Mater.* **2023**, *33*, 2210614.
[60] A. Kotikian, R. L. Truby, J. W. Boley, T. J. White, J. A. Lewis, *Adv. Mater.* **2018**, *30*, 1706164.
[61] W. Liao, Z. Yang, *Mater. Horiz.* **2023**, *10*, 576.
[62] H. Zeng, D. Martella, P. Wasylczyk, G. Cerretti, J.-C. G. Lavocat, C.-H. Ho, C. Parmeggiani, D. S. Wiersma, *Adv. Mater.* **2014**, *26*, 2319.
[63] J. Sandford O'neill, P. Salter, Z. Zhao, B. Chen, H. Daginawalla, M. J. Booth, S. J. Elston, S. M. Morris, *Adv. Optical Mater.* **2022**, *10*, 2102446.
[64] I. De Bellis, S. Nocentini, M. G. Delli Santi, D. Martella, C. Parmeggiani, S. Zanotto, D. S. Wiersma, *Laser Photonics Rev.* **2021**, *15*, 2100090.
[65] Y. Guo, H. Shahsavan, M. Sitti, *Adv. Mater.* **2020**, *32*, 2002753.
[66] S. Iamsaard, S. J. Aßhoff, B. Matt, T. Kudernac, J. J. L. M. Cornelissen, S. P. Fletcher, N. Katsonis, *Nature Chem* **2014**, *6*, 229.

© 2023 Wiley-VCH GmbH

2365709x, 0, Downloaded from https://onlinelibrary.wiley.com/doi/10.1002/admt.202300967 by Zhejiang University, Wiley Online Library on [04/10/2023]. See the Terms and Conditions (https://onlinelibrary.wiley.com/terms-and-conditions) on Wiley Online Library for rules of use; OA articles are governed by the applicable Creative Commons License